Received August 24, 2020, accepted September 9, 2020, date of publication September 18, 2020, date of current version October 8, 2020.

Digital Object Identifier 10.1109/ACCESS.2020.3024584

3D Printing of Millimetre Wave and Low-Terahertz Frequency Selective Surfaces Using Aerosol Jet Technology

ANSHUMAN SHASTRI[1], (Member, IEEE), BENITO SANZ-IZQUIERDO[1], (Member, IEEE), EDWARD A. PARKER[1], STEVEN GAO[1], (Fellow, IEEE), PATRICK REYNAERT[2], (Senior Member, IEEE), ZHIJIAO CHEN[3], (Member, IEEE), AND LEE WINCHESTER[4]

[1]School of Engineering and Digital Arts, University of Kent, Canterbury CT2 7NT, U.K.
[2]Department of Electrical Engineering (ESAT), Katholieke Universiteit Leuven, 3001 Leuven, Belgium
[3]School of Electronic Engineering, Beijing University of Posts and Telecommunications, Beijing 100876, China
[4]Centre for Process Innovation Ltd., Durham TS21 3FG, U.K.

Corresponding author: Benito Sanz-Izquierdo (b.sanz@kent.ac.uk)

This work was funded by UK Engineering and Physical Sciences Research Council (EPSRC) High Value Manufacturing Fellowship (REF: EP/L017121/1), the EPSRC grant titled Low-Profile Ultra-Wideband Wide-Scanning Multi-Function Beam-Steerable Array Antennas (EP/S005625/1), Royal Society - International Exchanges 2019 Cost Share (NSFC) (Ref: IEC\NSFC\191780) and CHIST ERA WISDOM project under EPSRC grant EP/P015840/1.

ABSTRACT An investigation of the use of Aerosol jet 3D Printing of frequency selective surface for millimetre and low-THz applications is presented in this article. This 3D printing technique allows the fabrication of intricate details of the designs with high resolution. Band-stop and band-pass FSS are designed and tested. The band stop FSS consisted of a Square loop array that operated in the 26-28 GHz sub-millimetre band. This design is printed on glass substrate and can be used for deployment in windows. The bandpass FSS arrays consisted of simple slot elements arranged in a square lattice and operated at 125 GHz and 280 GHz. The slot arrays were printed on Kapton. Surface profiles demonstrated the uniformity and precision of this printing technique. Simulated and measured results compared well and offered good performances at both the millimetre wave and low-THz bands. The designs find applications in 5G and imminent 6G communications. This printing technique also provides environmentally friendly, rapid, and sustainable alternative for development of highly customised FSS which can be deployed to improve communications in buildings and in future Terahertz applications.

INDEX TERMS Additive manufacturing, 3D printing, frequency selective surfaces, aerosol jet printing, electromagnetic wave propagation, millimetre-wave, terahertz.

I. INTRODUCTION

Frequency Selective Surfaces (FSS) are filtering devices for electromagnetic waves which are beneficial in a wide range of applications [1], [2]. FSS have traditionally been deployed in radomes [3], microwave absorbers [4], reflectors [5] and frequency demultiplexer [6]. Lately, FSS have found applications in control electromagnetic propagation in buildings [7], [8], remote sensing [9], beam steerable antennas, wireless communications [10]–[12] as well as gyro-multipliers [13]. FSS can be fabricated using of a variety of fabrication techniques such as etching [11], [12], [14], micromachining [15] and in more recent development, using additive manufacturing [16].

Additive manufacturing (AM), commonly known as 3D Printing is a popular technique that fabricates complex structures directly from their 3-Dimensional digital models [17]–[19]. 3D Printing breaks the 3D digital models into several thin layers and prints layer-by-layer. 3D printing is considered as an alternative to traditional methods and it has witnessed unprecedented growth in the past decade. Notable implementations of 3D printing are widespread and extended from fabricating mechanical components [20] to applications such as integrating electronic circuits within manufacturing [21], [22], antennas [23]–[27] and periodic electromagnetic structures [16], [28]–[38].

The associate editor coordinating the review of this manuscript and approving it for publication was Chinmoy Saha.

In terms of periodic EM structures, a variety of designs and techniques have been reported. Novel 3D structures are described in [28], [29] which use 3D printing of plasters with an additional layer of conductive material. This work was further expanded and utilized with Fused Deposition modelling (FDM) that reduced the resonant frequency by partially metalizing the hand painted conductive elements of the array [30]. 3D FSS developed using carbon reinforced plastic material was introduced in [31] where FDM using plastic polymer combined with Composite Filament Fabrication (CFF) techniques were utilized. 3D bandstop FSS with replaceable unit structures using Fused Filament Fabrication (FFF) was presented in [32]. 3D printed FSS made up entirely of dielectric elements operating at 10 GHz using stereolithography (SLA) is reported in [33]. 3D printing of metamaterial absorbers using AM techniques are reported in [33], [34] where a combination of AM techniques is employed. Broadband absorbers covering the X and K_u bands were fabricated using Selective Laser Sintering (SLS) using Nylon and Iron powder in [33]. The metamaterial absorber was printed with Ultimaker using PLA [34].

Inkjet printing using conductive silver nanoparticle ink is yet another lucrative technique which has been tested for producing FSS. Inkjet printing of frame dipole FSS was reported in [16] where a piezo inkjet printer was deployed to develop the dipoles. The technique has been demonstrated on textiles as well [35]. Further, mm-wave FSS filters are described in [36], [37] where inkjet printing of FSS operating at various millimetre wave frequencies was reported.

The AM FSS described above have largely been developed to operate in the microwave bands [16], [28]–[35], although some reported FSS also operate in millimetre wave bands [36]–[37]. With a rapid expansion and roll-out of 5G technologies along with the imminent arrival of 5G beyond and 6G technologies, low-THz designs will be significantly advantageous to help increase the signal strength and decrease the signal losses in near future.

This article evaluates the use of direct Aerosol Jet Printing in developing 3D Frequency Selective Surfaces for millimetre wave and low-THz applications. Aerosol jet printing produces reliable designs on thin, flexible substrates with millimetre to micrometre level precision. Tracks ranging from as low as microns to millimetres can be printed. It also allows for fabrication on curved, 3D and uneven surfaces [38] within the machine's limits. Bandstop and bandpass FSS are examined in this article. The bandstop design operates in millimetre wave bands and is intended for controlling EM waves in 5G communications. The FSS is printed using silver nanoparticle ink on glass for potential window installation. The bandpass FSS designs operate in the millimetre wave and low-THz bands and aimed primarily at future communications systems such as 6G and beyond.

The rest of the paper is arranged as follows: Section II presents the sub-millimetre wave bandstop square loop FSS design and the aerosol jet printing process. Section III presents a sub mm-wave 125 GHz Bandpass FSS design and section IV presents a low-THz 280 GHz bandpass FSS.

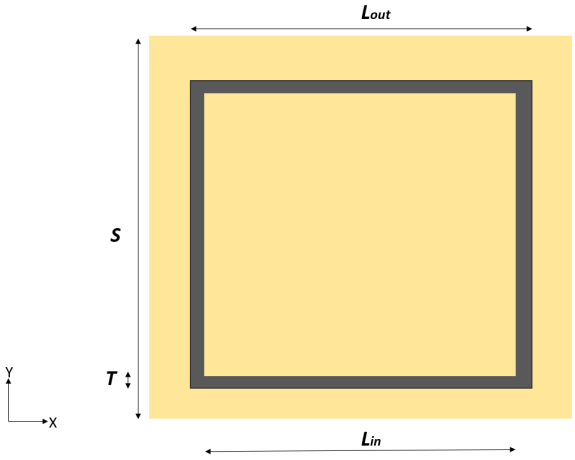

FIGURE 1. Square-loop patch FSS unit cell dimensions.

TABLE 1. Square loop patch FSS dimensions.

Parameters	L_{out}	S	T
Dimensions (mm)	2.7	3.4	0.42

II. SQUARE LOOP MILLIMETRE-WAVE BANDSTOP PATCH FSS DESIGN

A. SQUARE LOOP FSS DESIGN

Bandstop FSS arrays are capable of operating as screens to safeguard wireless devices from signal interferences. The square loop is a well-known FSS element which was first reported in [39], offers dual polarisation and good angle of incidence behaviours. They typically resonate when the perimeter of the loop is approximately one wavelength. Similar to the other types of filtering structures, the general equation for the resonant frequency of the square loop is expressed as:

$$\omega = \frac{1}{\sqrt{LC}} \tag{1}$$

where L and C relate to the dimensions and electrical properties of the conductive as well as dielectric components of a design.

An FSS consisting of an array of square loop elements in a square lattice was designed to operate at around 26 GHz. The configuration a square loop unit cell and corresponding dimensions can be seen in Fig. 1 and Table 1. The unit cell side length is denoted by S while the loop size is denoted by L_{out}. T denoted the thickness of the tracks and L_{in} was the difference between L_{out} and T. The unit cell was simulated using CST Microwave Studio^{TM} with glass as substrate. The thickness of the glass was 0.7 mm. The relative permittivity

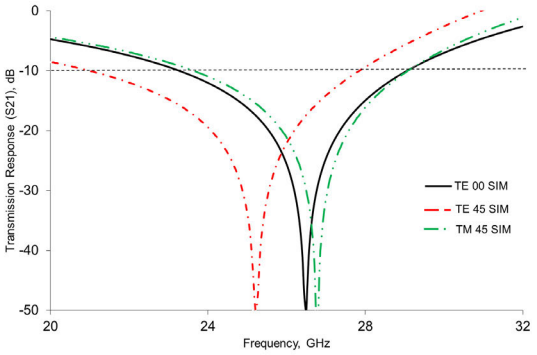

FIGURE 2. Simulated transmission response for square loop FSS design on glass.

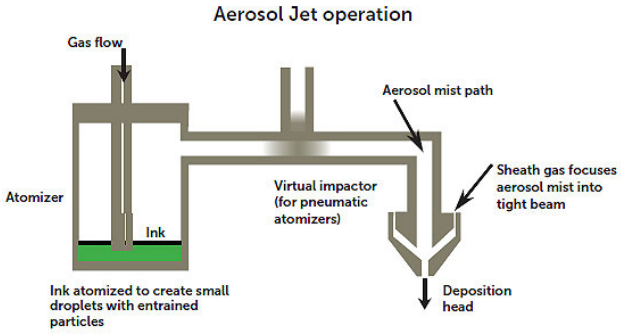

FIGURE 3. A typical Aerosol jet printer with its functions [45].

(ε_r) for Corning Eagle glass was 5.27 with a loss tangent of 0.001 [40], [41].

Fig. 2 shows the simulated transmission response of the FSS for angle of incidence behaviors at 0 degrees and 45 degrees, respectively. TE denotes the E-plane response whereas TM denotes H-plane response.

The design was not optimized for best angle of incidence performance but still provided a relatively good response. Further improvement in the transmission response at various angles of incidence could be achieved by reducing the distance between elements, using convoluted designs [42] and by selecting substrates with higher permittivity [42], [43]. The glass FSS operated at 26.7 GHz with a shift of approximately 5% at TE45 and 1% at TM45. Transmission response for glass at TE00 was below -10 dB for a range of 23.5 GHz to 29.2 GHz.

B. AEROSOL JET PRINTING

The FSS prototype was fabricated using Aerosol Jet printing that can fabricate designs with high precision [38], [44], [45]. A typical Aerosol Jet Printer layout can be seen in Fig. 3. The printing method uses aerodynamic focusing to deposit silver ink onto substrates in extremely precise and accurate manner. The ink is converted into a mist inside the atomizer. The mist is passed onto the deposition head where the mist is compressed with the help of sheath gas. Compressed air or Nitrogen are typically used as sheath gasses. As the sheath gas and

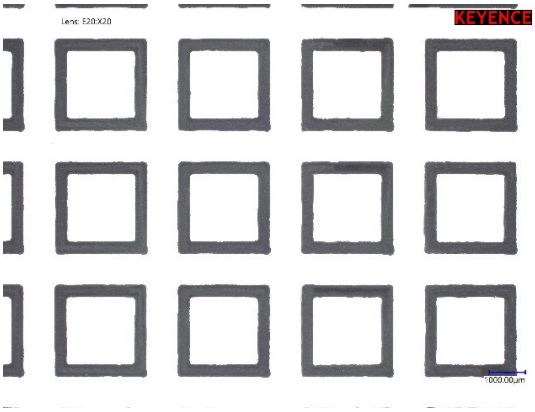

FIGURE 4. Printed FSS array layout of bandstop FSS.

ink aerosol are passed through the tiny nozzle, the aerosol is turned into an accelerated stream of droplets. The accelerated ink droplets and gasses exit the nozzle to travel and deposit onto the substrate. The height gap between the nozzle and the substrate typically varies between 2 to 5 mm, which provides the potential to print on non-uniform and 3D substrates within the limitations of the gap between the deposition head and substrates.

C. DESIGN PROFILES AND MEASUREMENTS

The FSS was printed using Cabot Nanoparticle silver ink [46], with the help of the equipment accessed through the Centre for Process Innovation, Durham, U.K. FSS array of 40 × 40 unit-cell elements was printed on a 200 mm×200 mm Corning Eagle glass of 0.7 mm thickness [40].

The design was cured with the help of dry heating to help the ink dry out and for the design to bind thoroughly across the substrate. The design was cured at a temperature of 180^0C for approximately 60 to 90 minutes. A magnified photograph of a 4×3 section of the fabricated array can be seen in Fig. 4. The photograph was taken using a Keyence® 4K Ultra HD microscope with 20x magnification. The photograph indicated the uniform printing of loops. The fabricated designs were further examined using Talysurf CCI optical interferometer with magnification factor of 50x and are shown in Fig.5. Measured surface profiles are presented in the figure where surface profile 3D map is presented in Fig. 5 (a) and cross-section view of the printed track is presented in Fig. 5 (b).

The surface profiles indicated a uniform deposition of loop elements and the coherence of printed dimensions with simulation values. The cross-section profile explained how the loops were printed as two loops, namely inner and outer loop and the ink spread across to form a single loop of desired dimensions. The calculated value of the resistivity of tracks was roughly 2.5×10^{-7} Ω-m which was consistent with the expected value for the Cabot nanoparticle silver ink [46]. Parameters for the roughness of the printed surface were obtained from interferometer for the FSS by taking an average

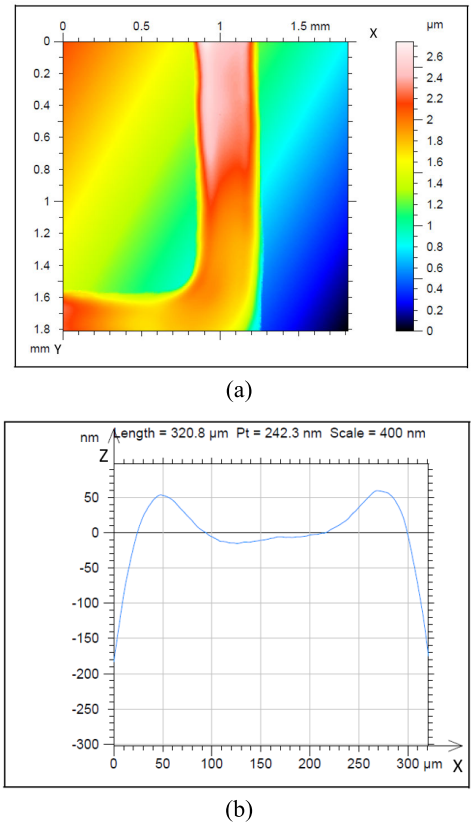

FIGURE 5. Surface profile measurement of FSS design from (a) Surface profile map and (b) lateral view where width is represented along X-axis and printed height is represented along Z-axis.

FIGURE 6. Measurement setup for the millimetre wave FSS design.

of all the measured sampling lengths. The FSS had an average surface roughness (Sa) value of 0.519 μm whereas the root mean square surface roughness (Sq) value was 0.627 μm. Measured average tolerance of $\pm 1\%$ was observed.

RF measurements were conducted using the standard transmission response measurement setup shown in Fig. 6. The setup consisted of two standard high gain log periodic transmitter and receiver antennas which were mounted either side of an absorber screen that can revolve around its axis to obtain different angles of incidence for measurements. The FSS was mounted on a piece of foam in a slot made within the screen. The remaining gap in the slot was filled with absorbers. Transmission responses were measured with the

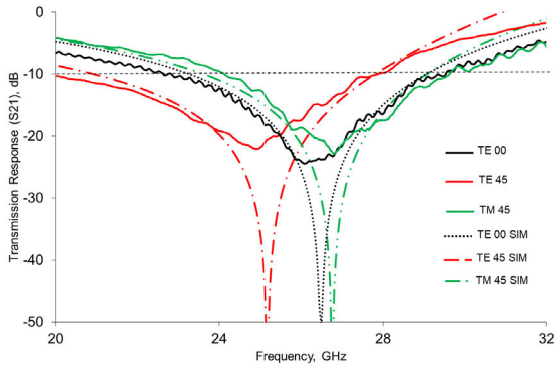

FIGURE 7. Transmission response of patch FSS design on glass.

help of Anritsu® 37397C Vector Network Analyzer (VNA) that operates up to 65 GHz, suitable for measurements at high frequencies. Transmitter and receiver antennas were positioned equidistant from the screen at 0.25 m from the FSS placed in the slot.

The measured transmission responses of FSS can be seen in Fig. 7 with their corresponding simulation responses. Normal wave incident angle response for FSS on glass resonated at a central frequency of 26.6 GHz. The transmission response was below -10 dB for a range from 22.9 GHz to 28.5 GHz with a bandwidth of 21%. TE45 response exhibited a shift of 8% whereas the TM45 response observed a shift of 1%. The transmission responses for FSS covered a range in the 26 GHz as well as the 28 GHz frequency bands which are highly sought-after bands of the 5G communication spectrum [47].

III. 125 GHz BANDPASS SLOT FSS DESIGN

A. SLOT FSS DESIGN

Bandpass FSS with filtering screens are widely used to realize wide-band frequency filtering responses [1]. Wideband transmission response of FSS with slot arrays makes them highly desirable for RF communication systems. Complementary dipole elements are well-known FSS elements that resonate when the slot length is approximately half wavelength in free space [1], [2].

An FSS consisting of an array of dipole slots arranged in a square lattice was designed to operate at a central frequency of 125 GHz. Fig. 8 and Table 2 correspond to the configuration and the dimensions of the unit cell. The unit cell consisted of length L and width W of 1 mm. The slots dimensions are denoted by L_s as 0.8 mm and W_s as 0.08 mm. The design was simulated using CST Microwave Studio™ using Kapton as substrate.

B. FABRICATION AND MEASUREMENTS

A slot FSS array consisting of a 50×50 grid of elements was printed on Kapton substrate [48] with dimensions of 63.5 mm×63.5 mm and a thickness of 0.05 mm [49]. Kapton was selected for its uniform permittivity value of 3.4 even at millimetre wave and sub-THz frequencies [48] and a loss

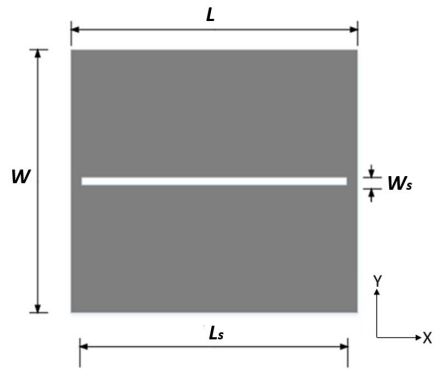

FIGURE 8. 125 GHz bandpass slot FSS unit cell layout.

TABLE 2. 125 GHz bandpass slot FSS dimensions (in mm).

Parameters	L_s	W_s	L	W
Dimensions (mm)	0.8	0.08	1	1

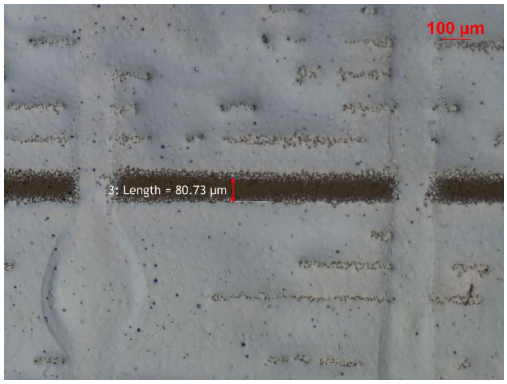

FIGURE 9. Fabricated FSS slot.

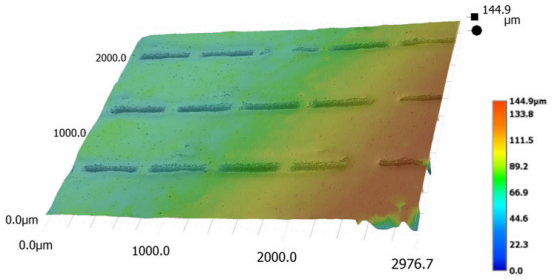

FIGURE 10. Measured 3D surface profile of FSS slots.

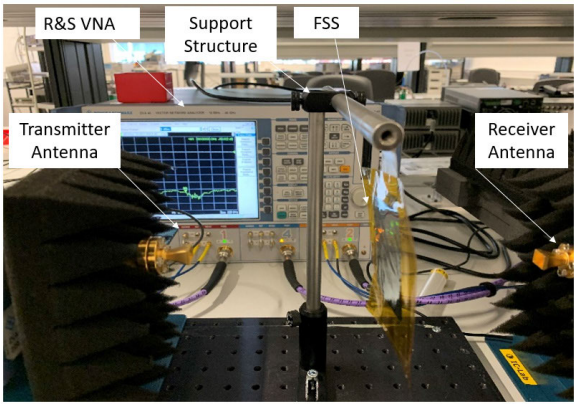

FIGURE 11. Measurement setup for transmission response. Some absorbers are removed for photo clarity.

tangent value of 0.002. The substrate is also resistant to high temperatures which makes it suitable for various applications in space communication. The slot array was printed by dividing the design into several subparts as per linear toolpath tracks and the printing process printed the subparts as a grid of long horizontal and vertical tracks.

The printed slot can be seen in Fig. 9. Horizontal tracks with gaps in between created the long apertures that constituted the slots while the vertical tracks determined the lengths of the slots and unit cells. A single-polarized FSS design was preferred as creating a toolpath and fabrication process was simpler with fewer fabrication constraints. A series of sample prototype prints were carried out by adjusting the stream of silver ink to produce the required dimensions. The width and length of printed slots deviated slightly around 0.08 mm and 0.8 mm. A width of 80.73 μm and a length 0.79 mm were observed at the points taken in the specific sample. Calculated value of resistivity of the printed surface on Kapton was $2.6 \times 10^{-7}\Omega$-m, which was similar to the results obtained for the glass substrate [46]. Detailed 3D profile of the slot array using a Keyence® 4K Ultra HD microscope is seen in Fig. 10. The maximum printed height was measured at approximately 45 μm. The measured Sa value was 0.202 μm while the Sq value was 0.246 μm. Measured tolerance average of $\pm 3\%$ was observed.

FSS was tested at the KU Leuven ESAT facility using the test setup for transmission response in Fig. 11. Absorbers around the FSS and supporting rods were removed for clarity of picture. The setup consisted of two horn antennas connected to the R&S Vector Network Analyzer with the help of frequency extenders. Some substrate area was left around the FSS for accessibility in handling the thin and flexible substrate for the duration of measurements. The FSS was mounted on a rotatable support structure.

The measurement transmission response is illustrated in Fig. 12. This FSS was designed and developed with the purpose of offering and analyzing the transmission response at normal angle of incidence and no further studies were carried out for other angles of incidence. As expected, the single-polarized FSS presented a passband response when H-plane incident wave was lateral (E-plane incident wave orthogonal) to the slot. A clear signal blocking state was observed when the E-plane was lateral to the slot. Transmission response at normal wave angle of incidence was centered at the resonant frequency of 125 GHz. Wideband transmission response with slow roll-off rate was observed with -10 dB passband ranging

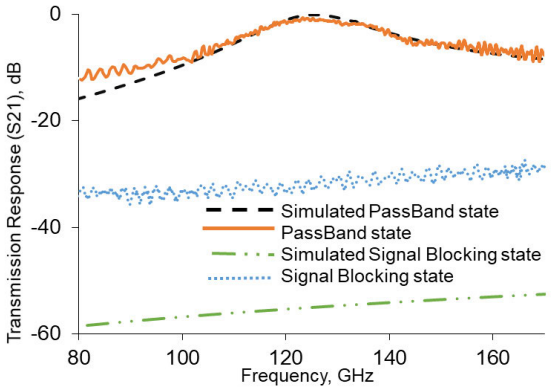

FIGURE 12. Transmission response at 125 GHz.

TABLE 3. 280 GHz bandpass slot FSS dimensions (in mm).

Parameters	L_s	W_s	L	W
Dimensions (mm)	0.43	0.04	0.6	0.6

from approximately 90 GHz all the way up to 170 GHz with a bandwidth of 64%. Insertion loss of 0.75 dB was observed. Single-band characteristics of FSS are highlighted with a gap of more than 20 dB between passband and signal blocking state. Good agreement was observed between simulated and measured transmission responses. Measured blocking state is 20 dB higher than simulations due to noise floor levels.

IV. 280 GHz BANDPASS SLOT FSS DESIGN

A. FSS DESIGN

A further analysis of the printing technique was carried out to develop low-THz bandpass FSS and the results are presented here. The design was analogous to the design demonstrated in Fig. 8. Dimensions of the low-THz design are presented in Table 3. The unit cell size was designed 40% smaller than the previous design and the slot size was roughly halved with L and W as 0.6 mm with slot length L_s of 0.43 mm and width W_s of 0.04 mm.

B. FABRICATION AND MEASUREMENTS

This FSS consisted of an array of 83×83 elements printed on Kapton [49] of an area of 6.35 cm×6.35 cm with 0.05 mm thickness. The tool path and deposition head speed for this FSS were drastically and regularly altered and modified throughout the fabrication process due to the sheer complexity and the extremity of this design. A photo of the printed FSS can be seen in Fig. 13. Dimensions of 0.43 mm×0.045 mm for one sample of the printed slot were observed. The dimensions of the printed slots were mostly consistent and on average varied close to the intended dimensions. 3D surface profile of one specific single slot using Keyence® 4K Ultra HD microscope is shown in Fig. 14.

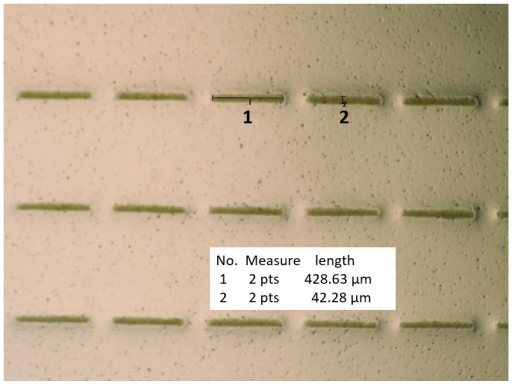

FIGURE 13. 280 GHz slot bandpass printed FSS layout.

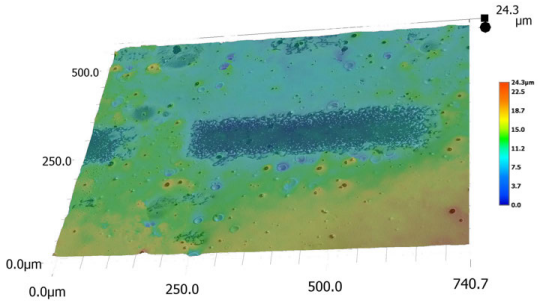

FIGURE 14. 3D Surface profile measurements of a single slot.

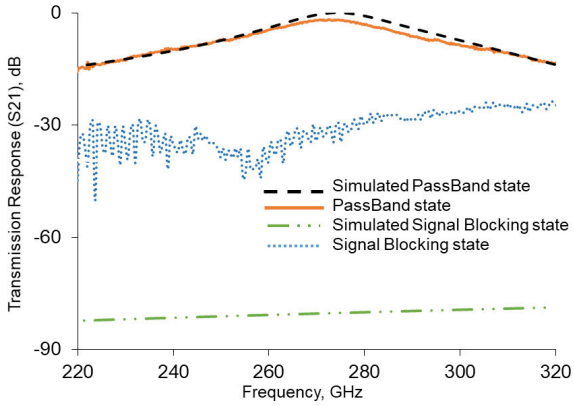

FIGURE 15. Transmission response at 280 GHz.

Surface roughness and height were comparable with the 125 GHz design. Average tolerance of ±5% was measured.

Measured setup for this FSS was same as seen in Fig. 11. Standard R&S transmitter and receiver horn antenna were mounted with frequency extenders to operate in the low-THZ frequency band.

The measured and simulated transmission response are presented in Fig. 15. The passband operated at a resonant frequency of about 280 GHz. A wideband transmission response was observed with -10 dB passband ranging from 240 GHz all the way up to 310 GHz with a passband bandwidth of approximately 28%. The slight shift in the

TABLE 4. Comparison table between some fabrication techniques reported for the development of frequency selective surfaces.

Fabrication Technique	Advantages	Disadvantages
Etching [14], [50]	• Cheapest • Scalable • Small features possible (1-4 µm track width) • Double-sided printing supported • Readily available • Reliable	• Multi-step fabrication • Requirements of stencils • Use of hazardous chemicals • Material and chemical wastage
Screen Printing [7]	• Scalable • Rapid printing speed • Small features possible • Possible printing on numerous substrates • Multilayer and intricate fabrication possible	• Multi-step process • Requirements of stencils • Poor three-dimensional resolution
Low-Cost Piezoelectric Inkjet printing [16], [36], [51]	• Low-cost equipment • No stencil required • Good resolution • Single-step fabrication • Environment Friendly • Rapid prototyping possible	• Not suited for mass production • Track size limitations (100~200 µm track width) • Cost-inefficient prices of ink • Mostly single-sided fabrication supported
Professional Inkjet printers [37], [51]	• No stencil required • High resolution • Repeatability (5 - 25 µm) • Well-suited with several materials and substrates • Fabrication on 3D substrates possible • Rapid prototyping possible	• High equipment cost • High fabrication cost • Unsuitable rate for bulk fabrication • Cost-inefficient prices of ink for scaling of production
Aerosol Jet Printers [44], [45], Proposed method	• Direct printing on 3D substrates within 2-5 mm height possible • No stencil required • Small feature possible (5 µm track width) • Extreme precision in fabrication • Suitable for mass production • Rapid prototyping possible	• High equipment cost, highest among the techniques mentioned • High fabrication cost (requires skilled operator) • Cost-inefficient prices of ink for scaling of production

response was caused by scattering of the deposition of ink marginally beyond the desired dimensions during the fabrication process. -10 dB bandwidth for the low-THz design was narrower in comparison to the 125 GHz design discussed earlier.

Measured and simulated transmission responses demonstrated a gap of about 20 dB between passband and signal blocking states. A measured insertion loss of approximately 2.4 dB was observed which was higher than the previous design as expected. Exceedingly high blocking response was observed in simulation but owing to the noise floor levels and the measurement constraints, a lower blocking state response is observed which is less than half of the simulated response. The response is still below -30 dB level and is a common occurrence for measurements of this sort. Overall, simulated, and measured transmission responses showed good relationship with each other.

Finally, a comparison table is presented in Table 4, comparing the advantages and disadvantages of various FSS fabricated using four popular techniques, namely etching, screen printing, low-cost and professional inkjet printing and Aerosol Jet printing. The table presents a list of essential characteristics of the various fabrication techniques used in developing an FSS and highlights the pros and cons of the fabrication methods. Aerosol Jet Printing presented an extremely precise, environment friendly fabrication alternative to the traditional methods with the potential to fabricate on non-planar substrates within the system constraints.

V. CONCLUSION

Aerosol Jet printing of Frequency Selective Surfaces ranging from sub mm-wave to low-THz frequency regions was demonstrated. The FSS were printed using an Optomec Aerosol Jet machine and nanoparticle silver ink. The fabrication of FSS was demonstrated on glass and Kapton substrates. Kapton was the preferred substrate at low-THz frequencies owing to the lower thickness of the substrate. Smooth surfaces and uniform conductivity of the printed layers of the designs were achieved. A bandstop FSS design for sub mm-wave and bandpass FSS designs for mm-wave and low-THz frequencies were proposed and studied. The bandstop FSS consisted of an array of square loops printed on glass and resonated at around 26.5 GHz. The FSS operated in the range from 24 GHz to 28 GHz which is extremely sought after in 5G and can be installed in windows for frequency shielding or to improve communications. The bandpass FSS were made up of slot arrays which were printed on Kapton and were tested at two frequencies: 125 GHz and 280 GHz.

The two designs tested the extremity and precision of aerosol jet printers and the insertion losses at the two frequencies. FSS design at 125 GHz offered a significantly wide −10 dB passband ranging from almost 90 GHz to 170 GHz with a bandwidth of 64%. Passband for 280 GHz design ranged from 240 GHz to 310 GHz with a bandwidth of 25%. More importantly, there was difference of approximately 20 dB between the passing states and the blocking states of the singly polarised designs. Developing dual-polarized bandstop design for sub mm-wave applications and single-polarized bandpass FSS structures for mm-wave and low-THz applications provided economical and uncomplicated solutions as a validation for their development. The manufacturing challenges in the dispersion of ink and in the development of the toolpath were addressed within this study. Kapton demonstrates extremely high temperature tolerance and finds applications in space and satellite communications. The initial studies for the sub-THz design can be developed further towards developing intricate and advance designs for ongoing 5G beyond and imminent 6G networks.

ACKNOWLEDGMENT

The authors would like to thank Dave Barwick and the CPI Staff for their assistance with fabrication, Alex Standaert from KU Leuven for his assistance with measurement setups, Mathew Armes from Keyence, and Dr. Mike Green from the University of Kent for their help with surface profile measurements.

REFERENCES

[1] B. A. Munk, *Frequency Selective Surfaces: Theory and Design*. New York, NY, USA: Wiley, 2000, pp. 636–659, doi: 10.1002/0471723770.

[2] E. A. Parker. (Jan. 1, 1991). *The Gentleman's Guide to Frequency Selective Surfaces*. Accessed: Jan. 1, 2020. [Online]. Available: https://kar.kent.ac.uk/59863/

[3] F. Costa and A. Monorchio, "A frequency selective radome with wideband absorbing properties," *IEEE Trans. Antennas Propag.*, vol. 60, no. 6, pp. 2740–2747, Jun. 2012, doi: 10.1109/TAP.2012.2194640.

[4] S. Chakravarty, R. Mittra, and N. R. Williams, "Application of a microgenetic algorithm (MGA) to the design of broadband microwave absorbers using multiple frequency selective surface screens buried in dielectrics," *IEEE Trans. Antennas Propag.*, vol. 50, no. 3, pp. 284–296, Mar. 2002.

[5] L. E. Comtesse, R. J. Langley, E. A. Parker, and J. C. Vardaxoglou, "Frequency selective surfaces in dual and triple band offset reflector antennas," in *Proc. 17th Eur. Microw. Conf.*, Oct. 1987, pp. 208–213.

[6] C.-C. Chang, R.-H. Lee, and T.-Y. Shih, "Design of a beam switching/steering butler matrix for phased array system," *IEEE Trans. Antennas Propag.*, vol. 58, no. 2, pp. 367–374, Feb. 2010.

[7] A. A. Dewani, S. G. O'Keefe, D. V. Thiel, and A. Galehdar, "Window RF shielding film using printed FSS," *IEEE Trans. Antennas Propag.*, vol. 66, no. 2, pp. 790–796, Feb. 2018, doi: 10.1109/TAP.2017.2780893.

[8] E. A. Parker, C. Antonopoulos, and N. E. Simpson, "Microwave band FSS in optically transparent conducting layers: Performance of ring element arrays," *Microw. Opt. Technol. Lett.*, vol. 16, no. 2, pp. 61–63, 1997, doi: 10.1002/(SICI)1098-2760(19971005)16:2<61::AID-MOP1>3.0.CO.2-G.

[9] B. G. Xia, C. F. Yao, J. Huang, J. Meng, D. H. Zhang, and J. S. Zhang, "Terahertz FSS for space borne passive remote sensing application," *Electron. Lett.*, vol. 49, no. 22, pp. 1398–1399, Oct. 2013, doi: 10.1049/el.2013.2407.

[10] L. Zhang, Q. Wu, and T. A. Denidni, "Electronically radiation pattern steerable antennas using active frequency selective surfaces," *IEEE Trans. Antennas Propag.*, vol. 61, no. 12, pp. 6000–6007, Dec. 2013, doi: 10.1109/TAP.2013.2282921.

[11] B. Liang, B. Sanz-Izquierdo, E. A. Parker, and J. C. Batchelor, "Cylindrical slot FSS configuration for beam-switching applications," *IEEE Trans. Antennas Propag.*, vol. 63, no. 1, pp. 166–173, Jan. 2015, doi: 10.1109/TAP.2014.2367534.

[12] C. Gu, B. S. Izquierdo, S. Gao, J. C. Batchelor, E. A. Parker, F. Qin, G. Wei, J. Li, and J. Xu, "Dual-band electronically beam-switched antenna using slot active frequency selective surface," *IEEE Trans. Antennas Propag.*, vol. 65, no. 3, pp. 1393–1398, Mar. 2017, doi: 10.1109/TAP.2016.2647578.

[13] X. Li, X. Liu, K. Ronald, W. He, Y. Zeng, Y. Alfadhl, R. Donnan, A. Cross, and X. Chen, "Investigation of frequency-selective surfaces for a THz gyromultiplier output system," *IEEE Trans. Electron Devices*, vol. 64, no. 11, pp. 4678–4685, Nov. 2017.

[14] M. Euler, V. Fusco, R. Dickie, R. Cahill, and J. Verheggen, "Sub-mm wet etched linear to circular polarization FSS based polarization converters," *IEEE Trans. Antennas Propag.*, vol. 59, no. 8, pp. 3103–3106, Aug. 2011, doi: 10.1109/TAP.2011.2158973.

[15] K. Kanjanasit and C. Wang, "A wideband resonant cavity antenna assembled using a micromachined CPW-fed patch source and a two-layer metamaterial superstrate," *IEEE Trans. Compon., Packag., Manuf. Technol.*, vol. 9, no. 6, pp. 1142–1150, Jun. 2019, doi: 10.1109/TCPMT.2018.2870479.

[16] B. M. Turki, E. T. A. Parker, S. Wunscher, U. S. Schubert, R. Saunders, V. Sanchez-Romaguera, M. A. Ziai, S. G. Yeates, and J. C. Batchelor, "Significant factors in the inkjet manufacture of frequency-selective surfaces," *IEEE Trans. Compon., Packag., Manuf. Technol.*, vol. 6, no. 6, pp. 933–940, Jun. 2016, doi: 10.1109/TCPMT.2016.2561972.

[17] D. Espalin, D. W. Muse, F. Medina, E. MacDonald, and R. B. Wicker, "3D Printing multifunctionality: Structures with electronics," *Int. J. Adv. Manuf. Technol.*, vol. 72, nos. 5–8, pp. 963–978, Mar. 2014.

[18] E. Macdonald, R. Salas, D. Espalin, M. Perez, E. Aguilera, D. Muse, and R. B. Wicker, "3D printing for the rapid prototyping of structural electronics," *IEEE Access*, vol. 2, pp. 234–242, 2014, doi: 10.1109/ACCESS.2014.2311810.

[19] K. Johnson, M. Zemba, B. P. Conner, J. Walker, E. Burden, K. Rogers, K. R. Cwiok, E. Macdonald, and P. Cortes, "Digital manufacturing of pathologically-complex 3D printed antennas," *IEEE Access*, vol. 7, pp. 39378–39389, 2019, doi: 10.1109/ACCESS.2019.2906868.

[20] C. K. Chua, K. H. Hong, and S. L. Ho, "Rapid tooling technology. Part 1. A comparative study," *Int. J. Adv. Manuf. Technol.*, vol. 15, no. 8, pp. 604–608, Jul. 1999.

[21] J. P. Desai, J. Sheng, S. S. Cheng, X. Wang, N. J. Deaton, and N. Rahman, "Toward patient-specific 3D-printed robotic systems for surgical interventions," *IEEE Trans. Med. Robot. Bionics*, vol. 1, no. 2, pp. 77–87, May 2019, doi: 10.1109/TMRB.2019.2912444.

[22] S. J. Leigh, R. J. Bradley, C. P. Purssell, D. R. Billson, and D. A. Hutchins, "A simple, low-cost conductive composite material for 3D printing of electronic sensors," *PLoS ONE*, vol. 7, no. 11, Nov. 2012, Art. no. e49365, doi: 10.1371/journal.pone.0049365.

[23] A. Shastri, S. Jun, B. Sanz-Izquierdo, H. Aldawas, Q. Ahmed, and M. Sobhy, "Evaluation of a low-cost inkjet printed slot antenna for energy harvesting applications," in *Proc. Loughborough Antennas Propag. Conf. (LAPC)*, Loughborough, U.K., Nov. 2016, pp. 1–5, doi: 10.1109/LAPC.2016.7807593.

[24] J. Heirons, S. Jun, A. Shastri, B. Sanz-Izquierdo, D. Bird, L. Winchester, L. Evans, and A. McClelland, "Inkjet printed GPS antenna on a 3D printed substrate using low-cost machines," in *Proc. Loughborough Antennas Propag. Conf. (LAPC)*, Loughborough, U.K., Nov. 2016, pp. 1–4, doi: 10.1109/LAPC.2016.7807590.

[25] S. Y. Jun, B. Sanz-Izquierdo, E. A. Parker, D. Bird, and A. McClelland, "Manufacturing considerations in the 3-D printing of fractal antennas," *IEEE Trans. Compon., Packag., Manuf. Technol.*, vol. 7, no. 11, pp. 1891–1898, Nov. 2017.

[26] S. Y. Jun, A. Shastri, B. Sanz-Izquierdo, D. Bird, and A. McClelland, "Investigation of antennas integrated into disposable unmanned aerial vehicles," *IEEE Trans. Veh. Technol.*, vol. 68, no. 1, pp. 604–612, Jan. 2019.

[27] R. Xu, S. Gao, B. S. Izquierdo, C. Gu, P. Reynaert, A. Standaert, G. J. Gibbons, I. Dmitry, W. Bosch, and M. E. Gadringer, "140 GHz additive manufacturing low-cost and high-gain Fabry–Perot resonator antenna," in *Proc. Int. Workshop Antenna Technol. (iWAT)*, Bucharest, Romania, Feb. 2020, pp. 1–4, doi: 10.1109/iWAT48004.2020.1570598322.

[28] B. Sanz-Izquierdo and E. A. Parker, "3D printing technique for fabrication of frequency selective structures for built environment," *Electron. Lett.*, vol. 49, no. 18, pp. 1117–1118, Aug. 2013, doi: 10.1049/el.2013.2256.

[29] B. Sanz-Izquierdo and E. A. Parker, "3-D printing of elements in frequency selective arrays," *IEEE Trans. Antennas Propag.*, vol. 62, no. 12, pp. 6060–6066, Dec. 2014, doi: 10.1109/TAP.2014.2359470.

[30] B. Sanz-Izquierdo and E. A. Parker, "Frequency selective surfaces formed by partially metalising 3D printed shapes," in *Proc. 9th Eur. Conf. Antennas Propag. (EuCAP)*, Lisbon, Portugal, 2015, pp. 1–4.

[31] R. Mirzavand, M. M. Honari, S. Aslanzadeh, H. Saghlatoon, and P. Mousavi, "Evaluation of one-staged 3-D printed frequency selective surface using carbon-fiber-reinforced thermoplastic composite," *IEEE Trans. Compon., Packag., Manuf. Technol.*, vol. 9, no. 11, pp. 2298–2304, Nov. 2019, doi: 10.1109/TCPMT.2019.2917197.

[32] S.-S. Cho, S.-H. Yoon, and I.-P. Hong, "Design of three-dimensional frequency selective structure with replaceable unit structures using a 3-D printing technique," *IEEE Antennas Wireless Propag. Lett.*, vol. 17, no. 11, pp. 2041–2045, Nov. 2018, doi: 10.1109/LAWP.2018.2871175.

[33] D. Zhou, X. Huang, and Z. Du, "Analysis and design of multilayered broadband radar absorbing metamaterial using the 3-D printing technology-based method," *IEEE Antennas Wireless Propag. Lett.*, vol. 16, pp. 133–136, 2017, doi: 10.1109/LAWP.2016.2560904.

[34] D. Lim, S. Yu, and S. Lim, "Miniaturized metamaterial absorber using three-dimensional printed stair-like jerusalem cross," *IEEE Access*, vol. 6, pp. 43654–43659, 2018, doi: 10.1109/ACCESS.2018.2862160.

[35] W. G. Whittow, K. Yang, Y. Li, R. Torah, J. Tudor, and S. Beeby, "Printed frequency selective surfaces on textiles," *Electron. Lett.*, vol. 50, no. 13, pp. 916–917, Jun. 2014, doi: 10.1049/el.2014.0955.

[36] O. Sushko, M. Pigeon, T. Kreouzis, C. Parini, R. Donnan, and R. Dubrovka, "Low-cost inkjet-printed FSS band-pass filters for 100 and 300 GHz," in *Proc. 10th Eur. Conf. Antennas Propag. (EuCAP)*, Apr. 2016, pp. 1–3, doi: 10.1109/EuCAP.2016.7481780.

[37] O. Sushko, M. Pigeon, R. S. Donnan, T. Kreouzis, C. G. Parini, and R. Dubrovka, "Comparative study of sub-THz FSS filters fabricated by inkjet printing, microprecision material printing, and photolithography," *IEEE Trans. Terahertz Sci. Technol.*, vol. 7, no. 2, pp. 184–190, Mar. 2017, doi: 10.1109/TTHZ.2017.2662582.

[38] S. Y. Jun, A. Elibiary, B. Sanz-Izquierdo, L. Winchester, D. Bird, and A. McCleland, "3-D printing of conformal antennas for diversity wrist worn applications," *IEEE Trans. Compon., Packag., Manuf. Technol.*, vol. 8, no. 12, pp. 2227–2235, Dec. 2018, doi: 10.1109/TCPMT.2018.2874424.

[39] R. J. Langley and E. A. Parker, "Equivalent circuit model for arrays of square loops," *Electron. Lett.*, vol. 18, no. 7, pp. 294–296, Apr. 1982.

[40] *Corning Eagle XG Glass datasheet*. Accessed: May 22, 2020. [Online]. Available: https://www.corning.com/media/worldwide/cdt/documents/EAGLE%20XG%20%20Slim%20Glass.pdf

[41] S. Chen, K. N. Nguyen, and M. N. Afsar, "Millimeter-wave dielectric permittivity of glasses," in *Proc. Joint 31st Int. Conf. Infr. Millim. Waves, 14th Int. Conf. Teraherz Electron.*, Shanghai, China, Sep. 2006, p. 406, doi: 10.1109/ICIMW.2006.368614.

[42] E. A. Parker, J. C. Batchelor, R. Chiang, A. G. Williamson, B. Sanz-Izquierdo, M. J. Neve, and K. W. Sowerby, "Frequency selectively screened office incorporating convoluted FSS window," *Electron. Lett.*, vol. 46, no. 5, pp. 317–318, Mar. 2010, doi: 10.1049/el.2010.2530.

[43] B. Sanz-Izquierdo, E. A. Parker, J.-B. Robertson, and J. C. Batchelor, "Singly and dual polarized convoluted frequency selective structures," *IEEE Trans. Antennas Propag.*, vol. 58, no. 3, pp. 690–696, Mar. 2010, doi: 10.1109/TAP.2009.2039321.

[44] *3D Printed Electronics—Aerosol Jet Technology—Optomec*. Accessed: May 7, 2020. [Online]. Available: https://optomec.com/printed-electronics/aerosol-jet-technology/

[45] L. Teschler. (2015). *Your Next Circuit Design Could be Fabricated on a Printer*. Design World. Accessed: May 22, 2020. [Online]. Available: https://www.designworldonline.com/your-next-circuit-design-could-be-fabricated-on-a-printer/

[46] L. Mo, Z. Guo, L. Yang, Q. Zhang, Y. Fang, Z. Xin, Z. Chen, K. Hu, L. Han, and L. Li, "Silver nanoparticles based ink with moderate sintering in flexible and printed electronics," *Int. J. Mol. Sci.*, vol. 20, no. 9, p. 2124, Apr. 2019, doi: 10.3390/ijms20092124.

[47] (2020). *Gsma.com*. Accessed: Jun. 21, 2020. [Online]. Available: https://www.gsma.com/spectrum/wp-content/uploads/2020/03/5G-Spectrum-Positions.pdf

[48] S. Sahin, N. K. Nahar, and K. Sertel, "Dielectric properties of low-loss polymers for mmW and THz applications," *J. Infr., Millim., Terahertz Waves*, vol. 40, no. 5, pp. 557–573, May 2019. 10.1007/s10762-019-00584-2

[49] *DupontTM Kapton HN Datasheet*. Accessed: May 22, 2020. [Online]. Available: https://www.dupont.com/content/dam/dupont/amer/us/en/products/ei-transformation/documents/DEC-Kapton-HN-datasheet.pdf

[50] O. Çakır, "Review of etchants for copper and its alloys in wet etching processes," *Key Eng. Mater.*, vols. 364–366, pp. 460–465, Dec. 2007, doi: 10.4028/www.scientific.net/kem.364-366.460.

[51] F. J. Romano, *Inkjet! Everything You Need to Know About Inkjet History, Technology, Markets, and Applications*. Warrendale, PA, USA: Printing Industries of America, 2012, pp. 37–179.

ANSHUMAN SHASTRI (Member, IEEE) received the B.E. degree (Hons.) in electronics and communications engineering from the Birla Institute of Technology and Science, Pilani, India, in 2014, and the M.Sc. by Research degree in electronics engineering from the University of Kent, U.K., in 2016.

He is currently a Ph.D. Researcher with the University of Kent. His research interests include microwave antennas, energy harvesting, additive manufacturing, frequency selective surfaces, millimetre wave devices, and modeling of frequency reconfigurable structures.

BENITO SANZ-IZQUIERDO (Member, IEEE) received the B.Sc. degree from the University of Las Palmas de Gran Canaria (ULPGC), Spain, and the M.Sc. and Ph.D. degrees from the University of Kent, U.K., in 2002 and 2007, respectively.

From 2003 to 2012, he was a Research Associate with the School of Engineering, University of Kent, where he became a Lecturer in Electronic Systems, in 2013, and a Senior Lecturer, in 2019. In 2012, he worked for Harada Industries Ltd., where he developed novel antennas for the automotive industry. His research interests include multiband antennas, wearable microwave devices, additive manufacturing, RF sensing, electromagnetic band-gap structures, and frequency selective surfaces.

EDWARD (TED) A. PARKER received the M.A. degree in physics and the Ph.D. degree in radio astronomy from the St. Catharine's College, University of Cambridge, Cambridge, U.K. He was appointed as a Reader with the University of Kent, Canterbury, U.K., in 1977, where he has been a Professor of Radio Communications, since 1987. He is currently a Professor Emeritus with the University of Kent. He established the Electronics Laboratory, Antennas Group, University of Kent. He is a member of the Livery of the Worshipful Company of Scientific Instrument Makers, London, U.K. His current research interests include the application of frequency selective surfaces and the study and overhaul of antique clocks. He is a member of the Institution of Engineering and Technology.

STEVEN GAO (Fellow, IEEE) received the Ph.D. degree in microwave engineering from Shanghai University, China, in 1999. He is currently a Full Professor and the Chair of RF and Microwave Engineering and the Director of Graduate Studies with the School of Engineering and Digital Arts, University of Kent, U.K. He has coauthored/coedited three books [*Space Antenna Handbook* (Wiley, 2012), *Circularly Polarized Antennas* (IEEE-Wiley, 2014), and *Low-Cost Smart Antennas* (Wiley, 2019)], over 300 articles, and ten patents. His research interests include smart antennas, phased arrays, MIMO, reconfigurable antennas, wideband/multiband antennas, satellite antennas, RF/microwave/mm-wave/THz circuits, mobile communications, satellite communications, UWB radars, synthetic-aperture radars, the Internet of Things (IoT), and sensors for healthcare. He is a Fellow of the Royal Aeronautical Society, U.K., and IET, U.K. He was the General Chair of LAPC 2013 and an Invited Speaker at many conferences. He is also an Associate Editor of the IEEE TRANSACTIONS ON ANTENNAS AND PROPAGATION and several other international journals, such as *Radio Science*, IEEE ACCESS, *Electronics Letters*, and *IET Circuits, Devices and Systems*, and the Editor-in-Chief of John Wiley and Sons Book Series on Microwave and Wireless Technologies. He was a Distinguished Lecturer of the IEEE AP Society.

PATRICK REYNAERT (Senior Member, IEEE) was born in Wilrijk, Belgium, in 1976. He received the Master of Industrial Sciences degree in electronics engineering from the Karel de Grote-Hogeschool, Antwerp, Belgium, in 1998, and the master's degree in electrical engineering and the Ph.D. degree in engineering science from the University of Leuven (KU Leuven), Leuven, Belgium, in 2001 and 2006, respectively. From 2006 to 2007, he was a Postdoctoral Researcher with the Department of Electrical Engineering and Computer Sciences, University of California at Berkeley, Berkeley, CA, USA, with the support of a BAEF Francqui Fellowship. In 2007, he was a Visiting Researcher at Infineon, Villach, Austria. Since October 2007, he has been a Professor with the Department of Electrical Engineering (ESAT-MICAS), KU Leuven. His current research interests include mm-wave and THz CMOS circuit design, high-speed circuits, and RF power amplifiers. He is also the Chair of the IEEE SSCS Benelux Chapter. He serves or has served on the Technical Program Committees of several international conferences, including ISSCC, ESSCIRC, RFIC, PRIME, and IEDM. He has served as an Associate Editor for the IEEE TRANSACTIONS ON CIRCUITS AND SYSTEMS—I: REGULAR PAPERS and a Guest Editor for the IEEE JOURNAL OF SOLID-STATE CIRCUITS.

ZHIJIAO CHEN (Member, IEEE) received the B.Sc. degree from the Beijing University of Posts and Telecommunications, in 2010, and the Ph.D. degree from the Queen Mary University of London, in 2014.

She joined the School of Electronic Engineering, Beijing University of Posts and Telecommunications, as a Lecturer, in 2014. She was on secondment to Ace-Axis Wireless Technology Laboratories Ltd., Essex, U.K., in 2012, and joined Northeastern University, Boston, MA, USA, as a Visiting Student, in 2013. Her research interests include dielectric resonator antennas, millimetre wave antennas, and 3-D printed antennas. She was a recipient of the Best Paper Award from iWAT 2013, Karlsruhe, Germany; the Third Prize Student Paper Competition from APS/URSI 2013, Orlando, FL, USA; the TICRA Travel Grant from EuCAP 2014, Hague, The Netherlands; and the Third Place from the QMUL Three-Minute Thesis (3MT) Competition Final 2014, London, U.K.

LEE WINCHESTER received the M.Sc. degree in nanotechnology and microsystems from Teesside University, Middlesbrough, U.K., in 2010. He is currently a Machine Engineer and a Printing Process Scientist with the Centre for Process Innovation Ltd., Durham, U.K. His current research interest includes the development of functional devices using aerosol jet deposition techniques.